Optical trapping of photochromic microcrystals by a dual fiber tweezers

K. Uchiyama, J. Fick, S. Huant, K. Uchida, M. Naruse, H. Hori

Optical trapping of photochromic microcrystals by a dual fiber tweezers

Kazuharu Uchiyama[1]*, Jochen Fick[2], Serge Huant[2], Kingo Uchida[3], Makoto Naruse[4] and Hirokazu Hori[1]

[1]*University of Yamanashi, 4-3-11 Takeda, Kofu, Yamanashi 400-8511, Japan*

[2]*University of Grenoble Alpes, CNRS, Institut Néel, 38000 Grenoble, France*

[3]*Ryukoku University, 1-5 Yokotani, Oe-cho, Seta, Otsu, Shiga, 520-2194, Japan*

[4]*Department of Information Physics and Computing, Graduate School of Information Science and Technology, The University of Tokyo, 7-3-1 Bunkyo-ku, Tokyo 113-8656, Japan*

Photochromic materials exhibit drastic changes in absorbance upon light irradiation: visible light makes them transparent (decolorization), whereas UV light makes them opaque (colorization). Their molecular structures vary with minute changes in molecular length or shape between the decolored and colored states, which induces differences in their mechanical properties. In this study, the optical trapping of photochromic microcrystals in both the decolored and colored states was successfully demonstrated using a dual fiber optical tweezers. Further, the reversible change of the trapping force by photoisomerization of the same single-crystalline piece was observed. The trapping stiffness in the axial direction for the colored crystal was approximately one-third of that for the decolored crystal, whereas that in the transverse direction was almost the same in both states. Such optical switching of optical trapping indicates the possibility of revealing the physical properties of trapped materials through trapping manners and can be applied to the physical computation of problems of high order difficulty.

Optical trapping has been intensively studied for various scientific and engineering purposes.[1–6] The objective of this technique is the trapping of small particles; therefore, the properties of the particles themselves are usually assumed to be constant over time during optical trapping. However, the addressability by light could dynamically configure the properties of the material under study, meaning that the method of optical trapping itself could be reconfigured. Conversely, the motion of the material under optical trapping dynamically changes its internal properties.

In this study, we succeeded in optically trapping photochromic microcrystals using near-infrared light while dynamically changing the absorbance of the photochromic material using external visible and ultraviolet (UV) light irradiation. Photochromic materials exhibit drastic changes in absorbance upon light irradiation: visible light irradiation makes them transparent (decolorization), whereas UV light makes them opaque (colorization). Here, we utilized a mi-

*E-mail: kuchiyama@yamanashi.ac.jp

crocrystal of photochromic diarylethene, which exhibits photoisomerization in the crystalline state.[7,8] The molecular structures vary with minute changes in molecular length or shape between the decolored and colored states,[9] meaning that the trapping force is different between these states. As for the photochromism of trapped objects, the trapping of a plastic particle including photochromic molecules was reported to show positional change via absorption switching of the trapping light.[10,11] In this study, we have realized the optical trapping of pure photochromic crystal by using off-resonant light with a dual fiber optical tweezers system so that we can separate the photoisomerization process from the trapping system and clearly evaluate the optical pressure and gradient force almost without absorption effect. In addition, by trapping the photochromic molecular crystal, we investigated the variation in trapping manner purely resulted from photoisomerization of the photochromic molecules without influence by other ingredients. This study demonstrates a novel composition of optical trapping and optical switching by using photochromic materials, providing a new means of producing functional optical devices and systems.

Diarylethene is a special photochromic molecule that can exhibit photochromism even in the crystalline state with thermal stability.[7] Fig. 1(a) shows the molecular structure of diarylethene **1o**.[12] The molecule **1o** is an open-ring state that is transparent to visible light and can be colored due to the molecular structure variation from **1o** to **1c** (closed-ring isomer) with UV light irradiation. Fig. 1(b) presents the absorption spectra of the two isomers in the crystalline state. The colored molecule can be decolored due to reverse isomerization to **1o** with visible light irradiation. We dissolved 1.2 mg of the diarylethene powder into 500 μL of isopropyl alcohol (IPA) and added 100 μL of it to water (1000 μL). In water, diarylethene microcrystals were generated after evaporation of IPA. After placing water containing the diarylethene microcrystals on a glass substrate, we observed the microcrystals on the glass using an optical microscope (Olympus, BX51M), as shown in Fig. 1(c). In addition, Fig. 1(d) provides an image of the microcrystal under study as observed by atomic force microscopy (AFM) (Bruker, Dimension Icon). Fig. 1(e) shows the height profile of the crystal observed by AFM along the solid white line depicted in Fig. 1(d). These images demonstrate that the crystal was circular with a radius of about 1 μm and that its thickness was approximately 100 nm. The refractive index of diarylethene crystals is reported to be approximately 1.55 – 1.6.[13]

The applied dual-fiber optical tweezers setup is described in detail elsewhere.[5] In short, two tapered optical fibers are mounted on two sets of piezoelectric translation stages for precise alignment (Fig. 2). The typical fiber-to-fiber distance is 10 μm. The chemically etched fiber tips have a Gaussian emission profile with an emission angle of 8°. For optical trapping, laser

light operated at a wavelength of 808 nm (Lumics, LU0808M250) was supplied through the two optical fiber probes. The actual laser power was 20 mW. The indicated light power was measured in air at the end of one single fiber and corrected for the higher emission efficiency in water. All measurements were done at room temperature in water.

Besides the trapping laser at 808 nm, three additional light sources were utilized (Fig. 2). Two LEDs emitting at 340 nm (Thorlabs M340L4) and 590 nm (M590L4) allowed us to colorize and decolorize the trapped photochromic microcrystals, respectively. A third LED emitting at 395 nm (M395L4) was used for particle trapping observation together with a large working distance microscope objective (Mitutoyo G Plan Apo 50x) and a CMOS camera (Hamamatsu, ORCA-Flash4.0LT). This setup enabled continuous observation of optically trapped single photochromic crystals dynamically configured to be either in the colored or in the decolored state.

The recorded trapping videos were used to determine the time-dependent crystal position. Each video frame was blurred with a Gaussian filter of 3 px (0.29 μm). The blurred images were then fitted to a two-dimensional Gaussian function. The trapping efficiency was determined by applying Boltzmann statistics (BS) in the framework of the equipartition theorem. The trapping potential $U(x)$ was determined by fitting[14)]

$$P(x) = Ne^{-\frac{U(x)}{k_B T}} \tag{1}$$

where $P(x)$ is the spatial trapped particle position distribution, N is the distribution constant, k_B is the Boltzmann constant, and T is the absolute temperature. Further applying the harmonic potential approximation $U(x) = 1/2\ k \cdot x^2$, one can define the trapping stiffness k.[5)]

Fig. 3(a) shows an optical microscope image of a trapped crystal and the two probe tips facing each other. The distance between the two fiber tips was 10 μm. The crystal was trapped near the midpoint between the two tips. Here, the crystal was in a decolored state. The disk shape of the crystal could not be resolved by our microscope with an estimated resolution of 500 nm. In order to characterize the trapping efficiency, we took a video of 5000 frames at 320 fps for approximately 15 s.

Figs. 3(b) and (c) depict the position records of the trapped crystal in the directions axial (x) and transverse (y) to the optical fiber axis, respectively. The motion range was approximately 2 μm in the axial direction and 1 μm in the transverse direction. Fig. 3(d) shows a scatter plot of the crystal $x - y$ positions over 5000 consecutive frames, and Fig. 3(e) presents the position histograms in x and y directions. Assuming that the trapping potential for the crystal is harmonic and constant during observation, the stiffness constants k were estimated to 22

fN/μm and 88 fN/μm in the axial and transverse directions, respectively.

Optical trapping is about four times more efficient in transverse than in axial direction. This large anisotropy is currently observed with dual beam tweezers and in particular with dual fiber tweezers.[5,15] It is explained by fundamental difference of the trapping scheme in each direction. When applying the common optical trapping models (ray optics model, or, electric dipole approximation model), the optical forces F_{opt} can be subdivided into the gradient force F_g and the scattering force F_s (See Supplementary data for electric dipole approximation).[16,17]

Optical trapping in the axial direction is governed by F_s which is some orders of magnitude higher than F_g. Trapping is produced by the equilibrium of the scattering forces caused by the two counter-propagating beams. A stable trap can, thus, only be realized for beams with varying central light intensities, such as diverging beams. In the transverse direction, F_s is negligible, and F_g attracts the particle to the center of the beams. The effect of both beams is adding up, thus explaining the higher trapping efficiency in the transverse direction.

Compared to trapping of 1μm polystyrene spheres with the same dual fiber tip tweezers setup,[5] the actual trap stiffness is about 10 times lower. The possible reason for the low force was the sample shape. The crystal thickness was approximately 100 nm, so the dimension was less than the light wavelength and is suitable for the electric dipole approximation; the crystal radius was approximately 1000 nm, which is longer than the light wavelength and is rather suitable for the ray optics model. The shape of the crystal needs to be treated intermediately with both models. First, in the electric dipole approximation, the force is proportional to the light intensity on the crystal. The small crystal volume causes the force to be low. Second, the shape is plate-like so that the variation of the light direction between the in and out timing is not large. In the ray optics model, the optical force on a sample is explained by the converse effect of the momentum change of the encountered light. Therefore, if the change in direction is small, the optical force caused by the light becomes small. In the model, the light traveling through the parallel face of the sample does not generate an optical force. In addition the scattering force by light reflexion depends on the orientation of the surface so that the effective light scattering is very different whether the light beam irradiates normal to the disk-shaped crystal surface or horizontally. These points provide the insight that the force depends on the sample direction. In the case of the sphere-shaped sample, the force is constant with sample rotation, but for the plate-shaped sample, the force is dependent on the sample direction. Thus, sample rotation affects the motion and trapping of the particle in the optical trapping system in the latter case. In the experimental system, the crystal is constantly

Table I. Measurement sequence.

Step	Feature	UV light	Vis. light	Durations	k_y	k_x
					$[\mathrm{fN}\cdot\mu\mathrm{m}^{-1}]$	
(1)	Observation of colored crystal	ON	OFF	20 s	77.3 ± 5.0	2.4 ± 0.2
(2)	Decolorization	OFF	ON	10 s	–	–
(3)	Observation of decolored crystal	OFF	ON	20 s	77.4 ± 3.8	7.8 ± 0.8
(4)	Colorization	ON	OFF	10 s	–	–
(5)	Observation of colored crystal	ON	OFF	20 s	69.1 ± 4.4	2.5 ± 0.4

subjected to random forces by water molecules, and the sample direction is expected to change drastically, which causes the variation of the trapping force and makes the trap stiffness low.

Next, we observed the dynamic changes of the photochromic crystals (that is, either colorization or decolorization) while keeping the crystal optically trapped. As the shapes of individual crystals are different, the mechanical properties differ depending on each crystal. Therefore, keeping the same crystal trapped is critical to examine the effects of photochromic switching induced in a particular crystal under observation. In addition, it is important to confirm the reversibility of photochromic switching to guarantee that the crystal is indeed the same and that the measurement and trapping conditions are nearly identical.

Observations were conducted continuously over 80 s, where 5000 frames in total were captured with a frame rate of 62.5 fps. Prior to measurement, the crystal was changed into a colored state by irradiating it with UV light. The measurement sequence consisted of five steps, including the three main observation steps and the two interval steps of decolorization/colorization, as depicted on Table I. All measurements were performed continuously to keep the same crystal trapped and under observation.

Fig. 4 summarizes the experimental observations in steps (1), (3), and (5), which correspond to the colored, decolored, and re-colored states of the photochromic crystal, respectively. For each step, a scatter plot of the sample position and histograms of the axial and transverse positions are depicted. In this measurement, the inter-tip probe distance was approximately 7 μm.

The transverse position range is approximately 1 μm for all steps. The axial position range is broader than that in the transverse direction and is not symmetric, especially with respect to steps (3) and (5). We estimated the trapping stiffness (k_x for the axial direction and k_y for the transverse direction) on the assumption that the position follows a Gaussian distribution. More accurate estimation is difficult at this stage, but a clear trend could be estimated in the

present study. Indeed, the distribution for the colored crystal [steps (1) and (5)] is broader than that of the decolored one [step (3)] in the axial direction. For steps (1) and (5) (colored crystal), the stiffness in the axial direction is approximately 2.5 fN/μm (Table I). For step (3) (decolored crystal), the constant is approximately 7.8 fN/μm, which is approximately three times larger than that of the colored crystal. Meanwhile, the trapping stiffness in the transverse direction was estimated to be 77.3, 77.4, and 69.1 fN/μm for steps (1), (3), and (5), respectively, indicating that there are no evident differences between the decolored and colored states.

Furthermore, we calculated the trapping stiffnesses based on the position information of the trapped crystal for shorter time of 10 s. Figs. 5(a) and (b) show the time evolution of the stiffness over time in the axial and transverse directions, respectively. These figures also indicate the durations corresponding to steps (2) and (4). We can clearly observe that the axial stiffness increases after decolorization and decreases after colorization in Fig. 5(a). On the other hand, the transverse stiffness is almost the same at all times (approximately 75 fN/μm), as observed in Fig. 5(b).

The potential energy structure was also determined from the histogram by Equation 1. We calculated $P(x)$ for the spatial range -3–3 μm with 50 bins for the axial (x-) and transverse (y-) axes (T is assumed to be 300 K). The estimated trapping potential energies for the three steps (Steps (1), (3), and (5)) are shown in Figs. 5(c) and (d) for the axial and transverse axes, respectively.

The potential shapes for the transverse direction in the three steps were simple and almost identical, which guarantees the stability of the laser light intensity and alignment as well as the sample temperature. For the axial direction, on the other hand, the bottom of the potential was flatter than the transverse potential, especially for the colored crystals (steps (1) and (5)), as shown in Fig. 5(c). The flatness is corresponding that the trapping stiffness was lower for the axial direction. And the potential shape was asymmetric for the axial direction. An asymmetric light intensity for the two fiber probe tips usually explains such an asymmetric shape. However, in this experiment, the light intensity was fixed during the entire measurement time. The bottom of the asymmetric potential was near the probe tip, which indicates an additional attractive force in the vicinity of the probe, especially for the decolored crystal. The strong repulsive force (optical pressure) from the probe tip and the additional attractive force make balance. The variable asymmetry in the obtained potential energy structures indicates that there are various stable positions for the trapped photochromic crystals in the axial direction, and the crystals are trapped temporarily in one of the stable

positions and hop between them.

The change in refractive index due to isomerization is usually a few percent,[13] which is too small to explain the large change in the axial (x-) axis potential or the change in the trapping stiffness constant. The change in shape is also a few percent or smaller but may have a significant effect on the trap because of the peculiar crystal shape of the thin disk. In addition, although the crystal structures of the open and closed rings of this material are identical, it is possible that mechanical distortions may occur in the particles in the intermediate state, resulting in a significant local change in the refractive index.

In conclusion, we demonstrated optical trapping of a photochromic microcrystal and performed decolorization and colorization of this microcrystal while the same crystal was optically trapped. Further, we succeeded in the reversible switching of the trapping stiffnesses, especially in the axial direction, induced by photoisomerization. The structure in the trapping potential and movement of particles on it can be applied to physical operations based on the positions of the particles. In addition, trapping multiple particles enables us to develop a calculation system using stochastic isomerization and changes in the stable trapping condition. The relation between trapping and the surrounding liquid is also important, and more diverse photoisomerization dependence may be observed if trapping is performed in liquids other than water.

Acknowledgment

This work was supported in part by the CREST program (JPMJCR17N2) of the Japan Science and Technology Agency and Grants-in-Aid for Scientific Research (JP26107012, JP17H01277, JP20H00233, and JP25286067) from the Japan Society for the Promotion of Science.

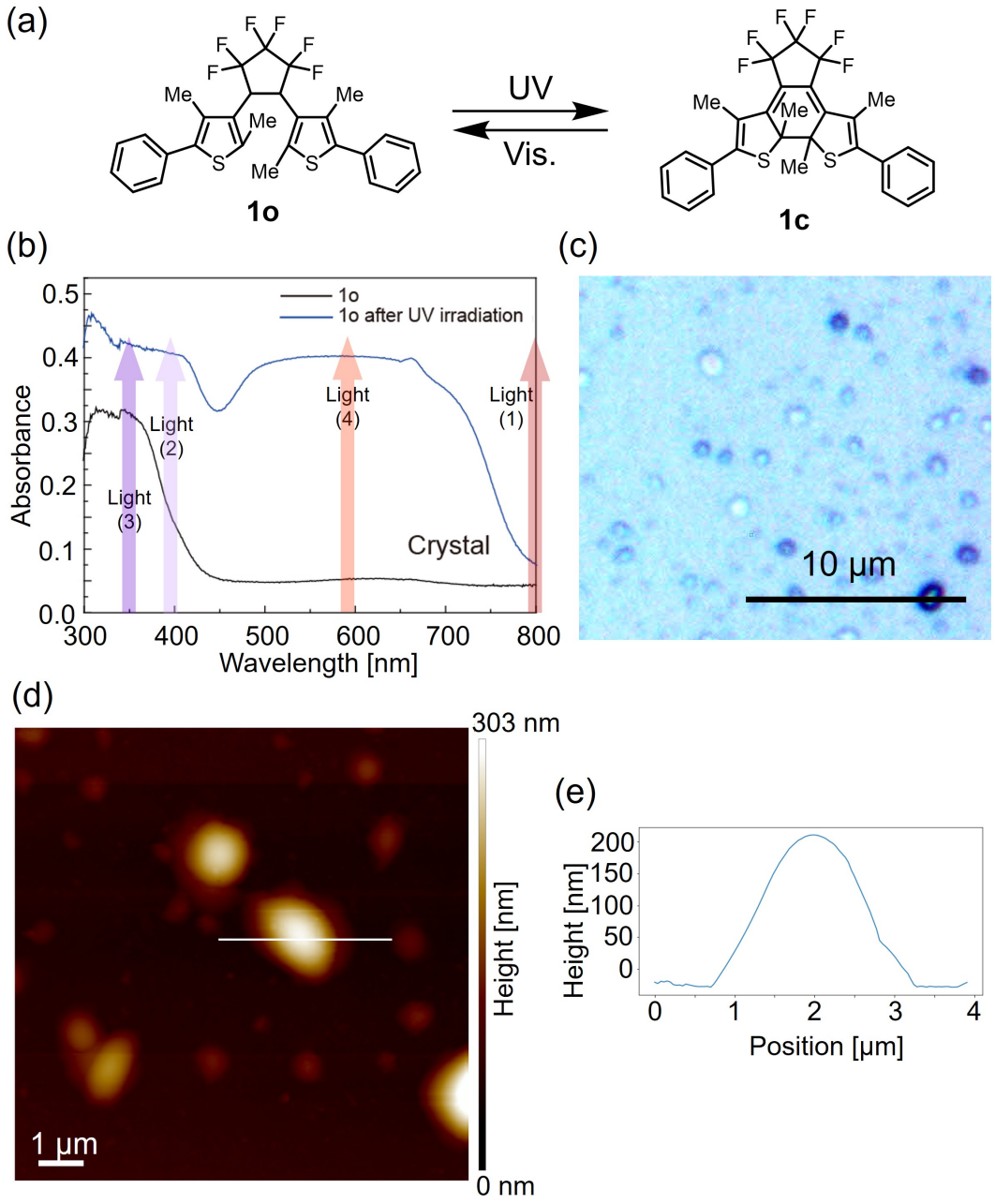

Fig. 1. (a) Open-ring isomer **1o** and closed-ring isomer **1c** of photochromic diarylethene used in this study. (b) Absorption spectra of the crystalline states of the diarylethene. The black and blue lines correspond to the open- and closed-ring isomers, respectively. Four wavelengths of lights used in this study are also indicated. Light(1) is for trapping; Light(2) is for observation; Light(3) is for colorization; Light(4) is for decolorization. (c) Optical microscope image of the diarylethene microcrystals. (d) AFM image of the microcrystals. (e) Line profile along the line shown in (d).

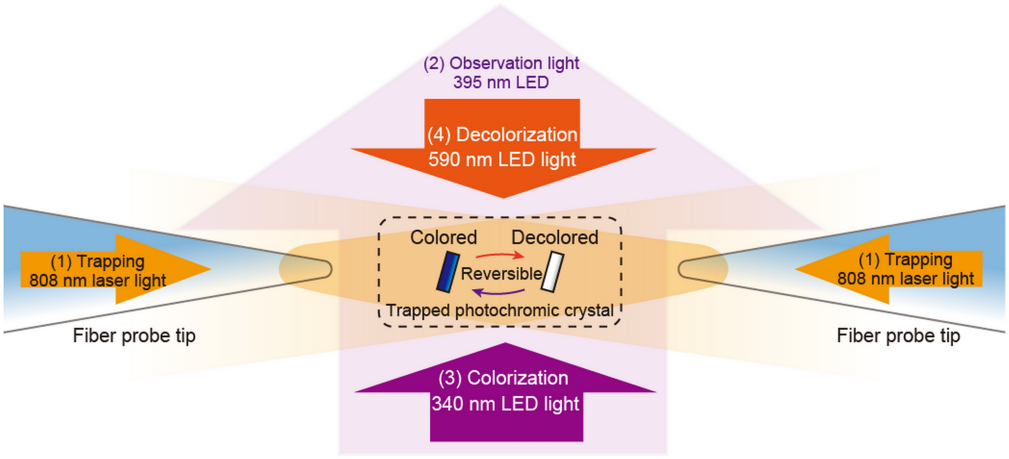

Fig. 2. Dual-fiber optical tweezers setup and light irradiation conditions. Five lights were set to be irradiated onto the trapped crystal. (1) Two lights with wavelengths of 808 nm set through optical fibers opposite to one another with a separation of several micrometers. (2) Observation light with a wavelength of 395 nm. (3) Colorization light with a wavelength of 340 nm. (4) Decolorization light with a wavelength of 590 nm.

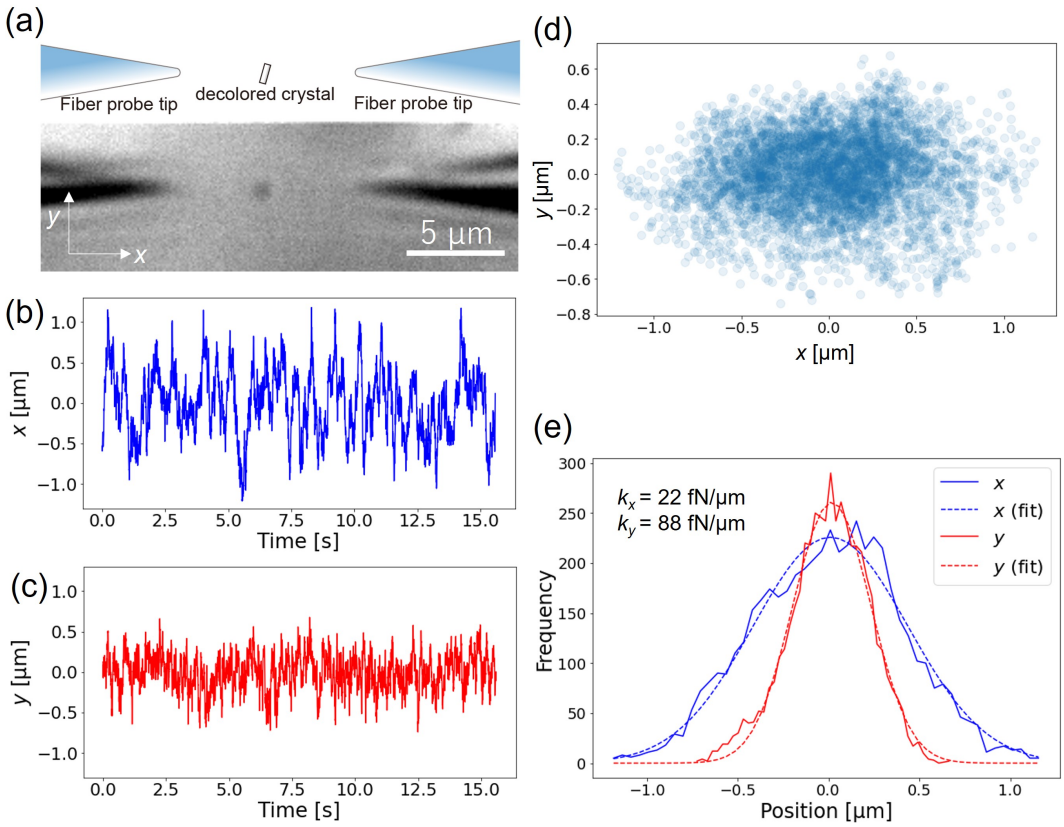

Fig. 3. Optical trapping of the decolored diarylethene microcrystal. (a) Schematic diagram of the experimental setup and optical microscope image. (b) Axial (x-axis) motion of the trapped microcrystal. (c) Transverse (y-axis) motion. (d) Scatter diagram of the position of the trapped microcrystal. (e) Histogram of the positions along the two axes and fitted curves, along with the estimated force constants.

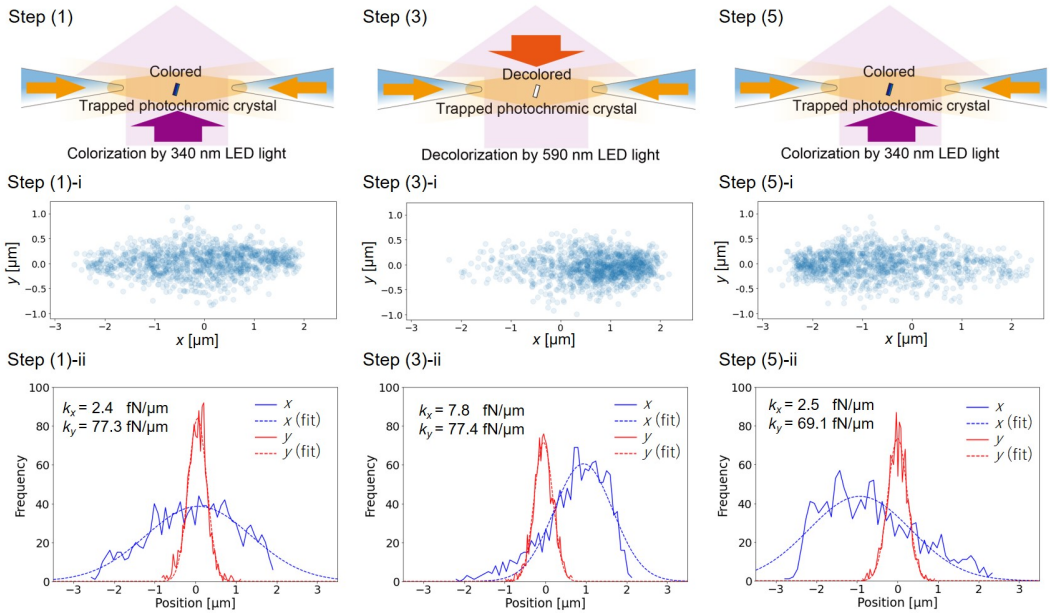

Fig. 4. Optical trapping of the same microcrystal for the two states (colored/decolored). Upper row: measurement conditions. Middle row: scatter diagrams of the position of the trapped crystal. Lower row: histograms of the x- and y-axis positions of the trapped crystal. The estimated trap stiffness constant for the two axes are shown in each figure. Left column: colored crystal (Step (1)). Middle column: decolored crystal (Step (3)). Right row: re-colored crystal (Step (5)).

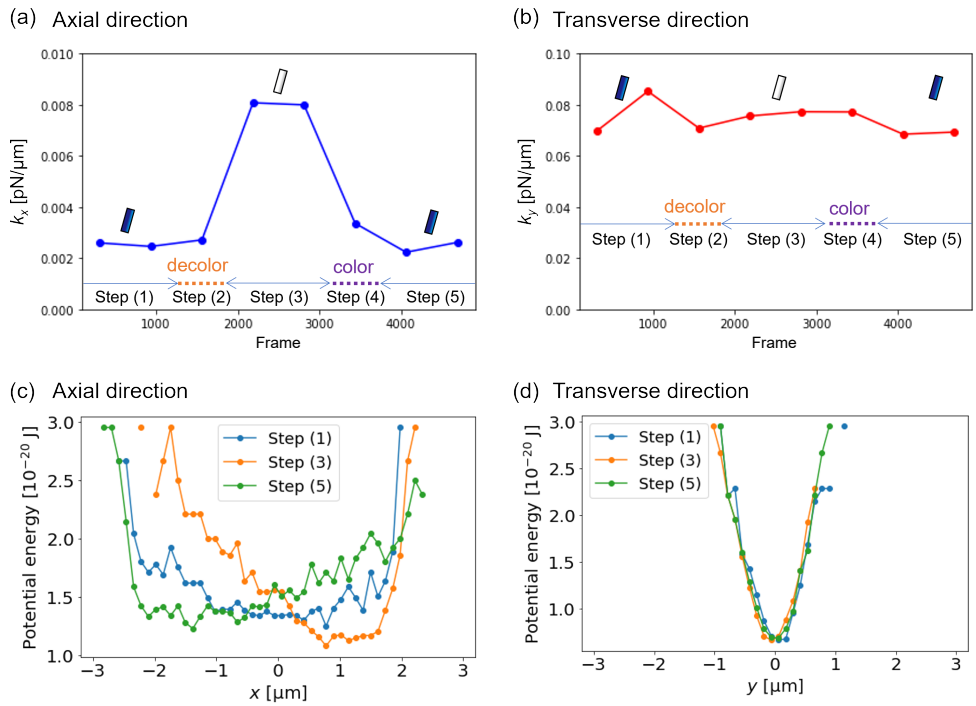

Fig. 5. (a) Axial and (b) transverse trapping stiffnesses for each 10 s (625 frames). Estimated trapping potentials for the two axes in the three measurement steps (Steps (1),(3), and (5))) for (c) the axial direction (d) the transverse direction.

References

1) A. Ashkin and J. Dziedzic, Science **235**, 1517 (1987)
2) K. C. Neuman andS. M. Block, Review of Scientific Instruments **75**, 2787 (2004)
3) P. J. Pauzauskie,P. J. Radenovic, E. Trepagnier, H. Shroff, P. Yang, and J. Liphardt, Nat. Mater. **5**, 97(2006)
4) Y. Pang and R. Gordon, Nano Letters **12**, 402 (2012)
5) J.-B. De-combe, S. Huant, and J. Fick, Opt. Express **21**, 30521 (2013)
6) C. Bradac, Adv. Opt.Mater. **6**, 1800005 (2018)
7) M. Irie, T. Fukaminato, K. Matsuda, and S. Kobatake,Chem. Rev. **114**, 12174 (2014)
8) M. Irie, Chem. Rev. **100**, 1685 (2000)
9) M. Irie, S. Kobatake, and M. Horichi, Science **291**, 1769 (2001)
10) S. Ito, M. Mitsuishi, K. Setoura, M. Tamura, T. Iida, M. Morimoto, M. Irie, and H. Miyasaka, J. Phys. Chem. Lett **9**, 2659 (2018)
11) K. Setoura, A. M. Memon, S. Ito, Y. Inagaki, K. Mutoh, J. Abe, and H. Miyasaka, J. Phys. Chem. C **122**, 22033 (2018)
12) M. Irie,K. Sakemura, M. Okinaka, and K. Uchida, J. Org. Chem. **60**, 8305 (1995)
13) T. Kawai, N. Fukuda, D. Groschel, S. Kobatake, and M. Irie, Jpn. J. Appl. Phys **38**, L1194(1999)
14) Y. Tanaka, A. Sanada, and K. Sasaki, Sci. Rep. **2**, 764 (2012)
15) A. Asadollahbaik, S. Thiele, K. Weber, A. Kumar, J. Drozella, F. Sterl, A. Herkom-mer, H. Giessen, and J. Fick, ACS Photonics **7**, 88 (2020)
16) M. Dienerowitz,M. Mazilu, and K. Dholakia, Journal of Nanophotonics **2**, 021875 (2008)
17) J.-B.Decombe, Ph.D. thesis, Grenoble University 2015.